Growth and Characterization of Large $CeAlO_3$ Perovskite Crystals

Pavel Arhipov[1], Sergii Tkachenko[1], Iaroslav Gerasymov[1], Oleg Sidletskiy[*,1], Kateryna Hubenko[1], Sergii Vasyukov[1], Natalia Shiran[1], Vyacheslav Baumer[2], Pavel Mateychenko[3], Alexey Fedorchenko[4], Yuriy Zorenko[5,6], Yaroslav Zhydachevskii[7,8], Kheirreddine Lebbou[9], Mikhail Korjik[10]*

[1]Institute for Scintillation Materials NAS of Ukraine, Kharkiv, Ukraine

[2]State Scientific Institution "Institute for Single Crystals NAS of Ukraine", Kharkiv, Ukraine

[3]Institute for Single Crystals NAS of Ukraine", Kharkiv, Ukraine

[4]Institute for Low Temperature Physics and Engineering NAS of Ukraine, Kharkiv, Ukraine

[5]Ivan Franko National University of Lviv, Gen. Tarnavskiy str. 107, 79017, Lviv, Ukraine

[6]Institute of Physics, Kazimierz Wielki University in Bydgoszcz, 85-064 Bydgoszcz, Poland

[7] Institute of Physics, Polish Academy of Sciences, Al. Lotników 32/46, 02-668 Warsaw, Poland

8 Lviv Polytechnic National University, Bandera str. 12, 79646, Lviv, Ukraine

[9]Institut Lumière Matière, UMR5306 CNRS, Universite de Lyon 1, 69622 Villeurbanne Cedex, France

[10]Research Institute for Nuclear Problems, Minsk, Belarus.

Corresponding Author: Oleg Sidletskiy, e-mail: sidletskiy@isma.kharkov.ua.

*Tel.: +380-57-341-0366. Fax: +380-57-340-4474

Abstract.

This study is focused on obtaining large $CeAlO_3$ single crystals. Using Czochralski and Edge-Defined Film Fed Growth techniques, crystals of length up to 130 mm were obtained. The crystals belong to the tetragonal low temperature modification of $CeAlO_3$, space group P4/mmm, a=3.7669Å, c=3.7967Å. Density and crystallographic parameters, as well as some optical, luminescence and magnetic properties of $CeAlO_3$ were studied. The crystals demonstrate rather bright luminescence under UV-excitation, while no luminescence has been registered under X-rays. Ceramic and single crystalline $CeAlO_3$ samples demonstrate p-type conductivity and promising paramagnetic properties.

KEYWORDS: A2.Single crystal growth, A2.Czochralski method, A2.Edge defined film fed growth, B1.Perovskites, B1.$CeAlO_3$, A1.Luminescence.

1. Introduction

Perovskite-type rare earth (RE) and yttrium aluminate oxide single crystals $REAlO_3$ are widely applied laser, magnetooptical and scintillating materials. For example, Ce^{3+} and Pr^{3+}-doped $YAlO_3$ and Ce^{3+}-doped $GdAlO_3$:Ce are bright and fast scintillators [1].

Technologies of $REAlO_3$ crystal growth have been extensively developed. Despite very high melting temperatures up to 2370 K, such crystals are potentially low cost due to possibility of

their growth in Mo or W crucibles [2] instead of Ir. $REAlO_3$ compounds (R = Dy-Lu and Y) adopt orthorhombic symmetry and the $GdFeO_3$ structure type and have no confirmed structural transitions between room temperature (RT) and their melting point [3]. They can be obtained rather easily in the form of bulk crystals by direct crystallization from the melt by the Czochralski or Bridgman techniques. Cerium doped yttrium aluminum perovskite (YAP:Ce) single crystals have the most developed growth technology and are commercially produced. Compounds of the $REAlO_3$ series (R = Dy-La) with larger RE ionic radius exhibit structural transitions between RT and the melting point [2]. As a result, single crystals of the latter group of compounds are prone to cracking. $CeAlO_3$ is among the most complex systems from this group. It has 3 polymorph transitions in the temperature range between 273 and 1373 K. In accordance with [4] the sequence of transitions is as follows: tetragonal *I*4/*mcm* (up to 314 K), orthorhombic *Imma* (314 - 431 K), rhombohedral $R\bar{3}c$ *(431 - 1223 K)*, cubic $Pm\bar{3}m$ (>1223 K). In addition, the formation of a metastable, hexagonal form of $CeAlO_3$ at 1120-1170 K, isomorphous to the hexagonal $LnAlO_3$ polymorph for heavy lanthanides and Y, has been reported recently [5].

An interest in $CeAlO_3$ crystals is caused by their ferroelectric, optical, and luminescence properties, and the possibility to apply them as solid electrolytes, gaseous gauges, and catalysts [6]. The majority of data on $CeAlO_3$ properties have been obtained on powders or ceramics prepared by solid state synthesis. Single crystals have not been studied in detail. Crystals with similar structure transitions - $LaAlO_3$:Ce,Sr,Ti, $PrAlO_3$, $PrAlO_3$:Ce,Sr, $Pr_xLa_{1-x}AlO_3$ - were grown by different methods [7-11]. $CeAlO_3$ crystals with length 5 mm and 3 mm diameter were obtained by direct induction melting and cooling in a cold crucible [7]. Growth of $CeAlO_3$ single crystals from melt-solution using a KF flux was reported in [8-10] –transparent cubic crystals of pale yellow color with 300-600 μm dimensions were crystallized over a period of eight days.

To our knowledge, there have been no reports on growth or study of bulk $CeAlO_3$ single crystals. This work is focused on the growth and characterization of large $CeAlO_3$ crystals grown from the melt by the Czochralski and EFG (Edge-Defined Film-Fed Growth) techniques.

2. Experimental section

2.1. Solid state synthesis

Cerium oxide is commercially available in the tetravalent state, but Ce^{3+} ions are in the trivalent state in $CeAlO_3$, so the $CeAlO_3$ raw material should be prepared with the following reaction:

$2CeO_2 + Al_2O_3 = 2CeAlO_3 + 1/2O_2$.

CeO_2 and Al_2O_3 powders with 4N purity were used for the solid state reaction. The synthesis temperature was controlled using a Raytek Marathon MM2MHVF1V pyrometer. Elemental composition of the tablets was measured using a JSM 6390 LVX scanning electron microscope equipped with MAX^N X-ray microanalysis system. Structure and phase composition was determined with a Siemens D500 diffractometer.

2.2. Crystal growth

$CeAlO_3$ single crystals were grown by the Czochralski and EFG techniques with induction radiofrequency heating in an atmosphere of Ar with 6N purity. First crystals were obtained by the Czochralski technique by seeding onto Mo or W wire. The crystals were grown from a W crucible with inner diameter 45 mm, the pulling rates 1.5-15 mm/hour, and the rotation rates 0-20 rpm. A reducing atmosphere was formed after melting the raw material and melt evaporation due to reaction of the oxides with graphite heat insulation with subsequent CO gas formation.

During EFG growth we used Mo shapers: a 12 mm round shaper with a central supply channel for growth of cylindrical rods, and a 20x3 mm^2 size rectangular shaper for growth of plates. The rods and plates were grown at a rate of 10-12 mm/hour using fragments of Czochralski-grown crystal as the seeds.

2.3. Determination of optical properties

Excitation and emission spectra, as well as absorption spectra and luminescence decay curves, were measured on samples with 1-2 mm thickness with polished faces. The absorption spectra were measured in the range of 190 – 1100 nm using a Specord 40 spectrophotometer (Analytik Jena AG). Excitation and emission spectra in the 230–800 nm range were determined using a combined fluorescent lifetime and steady-state spectrometer FLS 920 (Edinburgh Instruments) equipped with a Xe lamp for steady-state measurements. The photoluminescence (PL) decay kinetics were registered using a Horiba/Jobin-Yvon Fluorolog-3 spectrofluorimeter with Horiba nano-LEDs for excitation and a Hamamatsu R928 photomultiplier. All measurements were carried out at room temperature.

2.4. Study of magnetic properties

Magnetic properties of polycrystalline and single crystalline $CeAlO_3$ samples were studied using a SQUID magnetometer [11, 12] in the temperature range 4.2 - 290 K. The maximum linear dimensions of the studied samples did not exceed 6 mm. Temperature dependencies of magnetic susceptibility $\chi(T)$ were recorded after cooling down to liquid He temperature without magnetic field with subsequent application of magnetic field H = 10.2 Oe and slow heating at a rate of 1.5 K/min.

3. Crystal growth.

3.1. Optimization of raw materials preparation procedure

We have to choose optimal conditions of synthesis based on the properties of the starting materials and features of the graphite thermal insulation. The starting powders were mixed, pressed, dried, and calcined in a weakly reducing atmosphere, Ar+CO, at 1920-2070 K for periods of 10-60 hours. The reducing atmosphere was created with the aim to reduce cerium into the trivalent state. Under optimized conditions we obtained polycrystalline $CeAlO_3$ of pale yellow color (Fig. 1) with tetragonal structure, space group *I*4/mcm, while crystals with other habits were formed in the sample as well. Fig. 1 shows cubic, hexagonal and more complex faceting. Synthesized ceramic tablets of $CeAlO_3$ were then used as raw materials for Czochralski and EFG processes.

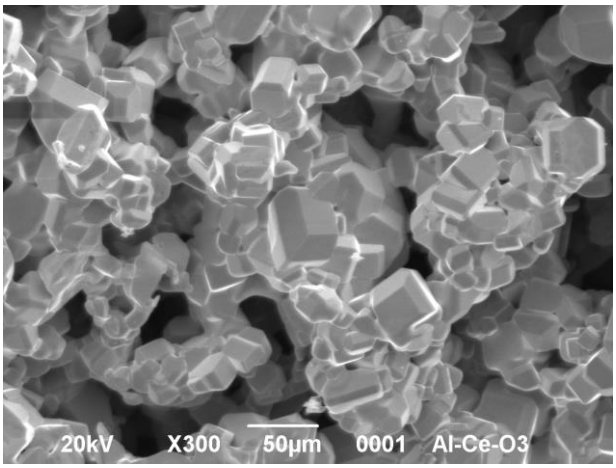

Fig. 1. Microscopic view of polycrystalline $CeAlO_3$.

3.2. Czochralski growth

Cerium perovskite crystallizes in the Al_2O_3 - Ce_2O_3 binary system at 2348 K [13]. The high melting point imposes limitations on the choice of crucible material – Ir, Mo, Rh, or W. During $CeAlO_3$ crystallization, the crucible surface may heat above 2600 K, which is dangerous for Ir. Mo forms a eutectic with Mo_2C at 2470 K [14], and Rh is very expensive. Therefore, comparably cheap tungsten with very high melting point at 3683 K was chosen as the crucible material. Crystals with diameters up to 30 mm grown by the Czochralski technique from a W crucible were dark-green or yellow (Fig. 2). According to XRD their structure was tetragonal, space group P4/mmm, with lattice parameters a=3.7669Å and c=3.7967Å, similar to those published in [7, 8].

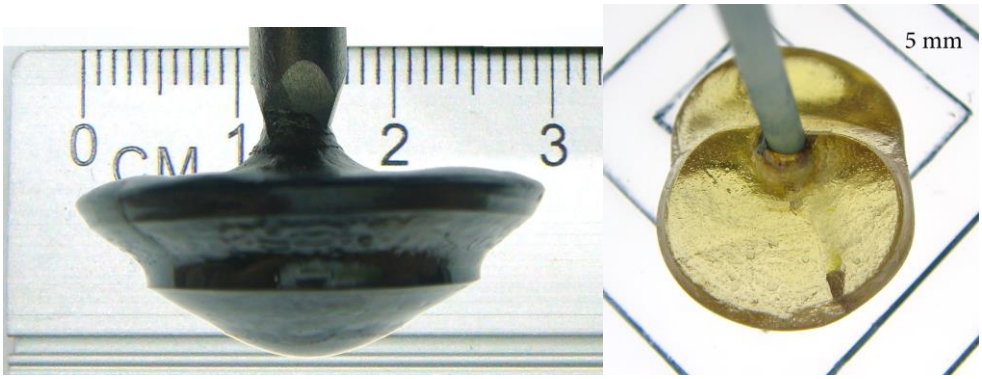

Fig. 2. As grown $CeAlO_3$ single crystals obtained by the Czochralski technique.

We did not succeed in growing cylindrically shaped crystals by varying different growth parameters. Starting at a certain length the crystals began to grow along the melt surface and then their shape transformed into a screw. The unstable growth is caused by the low thermal conductivity of these perovskites [15] and a large melt meniscus. During our experiments, the height of the meniscus was ~ 3 mm. Good wetting of Mo and W by the $CeAlO_3$ melt showed a possibility to use EFG technique during further experiments.

Because of evaporation, a deposit accumulated on the seed holder and chamber walls. The total melt losses from evaporation during the crystal growth were 5-10 % wt. Phase analysis showed that this deposit consists of $CeAlO_3$ with admixtures of carbon, Ce_2C_3 and Al_2O_3. After some experiments we observed dendrite and skeleton $CeAlO_3$ crystals formed on the seed holder and heat shields (Fig. 3). These crystals are not colored and are visually transparent. According to XRD analysis, dendrites and skeleton crystals are tetragonal $CeAlO_3$, space group *I*4/mcm.

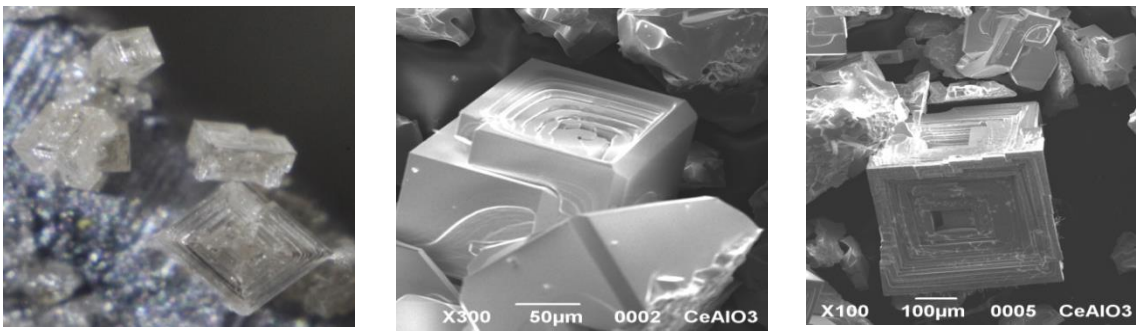

Fig. 3. $CeAlO_3$ skeleton crystals.

The observed crystallization of $CeAlO_3$ from the gaseous phase becomes possible at congruent evaporation of the melt. Such character of evaporation minimizes the melt non-stoichiometry during the growth process and is of great advantage in obtaining good quality crystals. Such character of evaporation also points to the possibility of $CeAlO_3$ thin film deposition in vacuum.

3.3. EFG technique

Compared to the Czochralski technique, in the EFG process it is possible to create a higher thermal gradient at the crystallization interface, and to achieve real-time observation of the growing crystal and crystallization interface shapes. The disadvantages of EFG comprise a high sensitivity

to admixtures in the melt and the melt non-stoichiometry. Excess of one of the components or too high an admixture content in the meniscus results in a crystallization temperature decrease (constitutional undercooling) and leads to unstable growth due to changes in wetting and surface tension.

Plates with length up to 80 mm obtained by the EFG technique were yellow and yellow-green (Fig. 4), just like the Czochralski grown crystals. Such coloration is caused by intense segregation of admixtures to the surfaces of the plates, which is inherent to EFG. Admixtures may be comprised of the excessive Ce_2O_3, Al_2O_3, or they can be created by interaction of the melt with CO in the growth chamber. Color centers and gaseous inclusions in crystals were concentrated on the surface layer, but the inner bulk region was transparent with no visible macrodefects.

Fig. 4. As-grown crystalline plate obtained by the EFG technique.

The EFG method was also applied to grow cylindrical rods with diameter 12 mm and length up to 130 mm (Fig. 5). After thermal annealing in a reducing atmosphere and vacuum they became pale yellow and green, respectively. The crystal coloration changes are reversible and depend on the atmosphere composition.

a

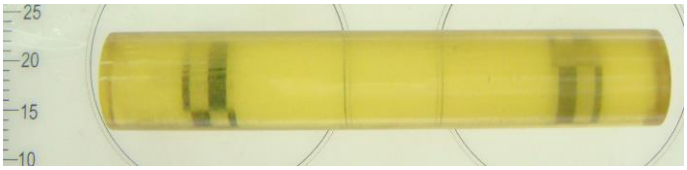

b

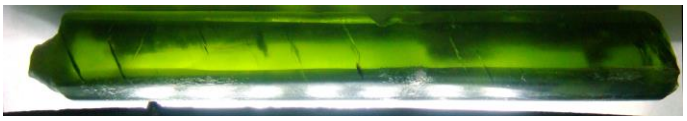
c

Fig. 5. $CeAlO_3$ crystals obtained by the EFG technique: as-grown (a), heat treated in reducing atmosphere and polished (b), heat trated in vacuum and polished (c).

4. Properties of $CeAlO_3$

Since bulk crystals had not been obtained previously, only calculated data on $CeAlO_3$ density have been published - 6.64 g/cm^3 [16] and 6.62 g/cm^3 [17]. In the present work, a density of 6.69 g/cm^3 was determined by hydrostatic weighting. The melt density was evaluated as 5±0.1 g/cm^3 by choosing optimal parameters for automated crystal growth by the weight sensor control.

4.1. Optical properties

Absorption spectra of crystals grown by the EFG technique are presented in Fig. 6. Yellowish crystals are transparent from ~400 nm. The absorption spectra of $CeAlO_3$ crystals are resolved into three separate bands peaked at 331, 360 and 380 nm and a wide band peaked at 227 nm. They can correspond to the 4f – 5d^1 ($^3T_{2g}$ and ^2E) transition of Ce^{3+} ions in the perovskite [18] or crystallographically similar hosts, such as $CeAl_{11}O_{18}$ phase inclusions. As one can see from Fig. 6, the fundamental absorption edge of $CeAlO_3$ crystals lies below 180 nm (usually below 150 nm in the perovskite host) [18].

In greenish $CeAlO_3$ crystals the short wavelength edge of optical transmission is strongly shifted to ~500 nm. The difference in the absorption spectra of greenish and yellowish $CeAlO_3$ crystals shows the addition of a strong band peaked at 400 nm and a bump at 300 nm. The last band may be related to O^{2-} - Ce^{4+} charge transfer transitions [18]. Since the samples turn yellow under heat treatment in a reducing atmosphere and become deep green in an oxidizing atmosphere, the coloration change is probably related to the $Ce^{3+} \leftrightarrow Ce^{4+}$ recharging.

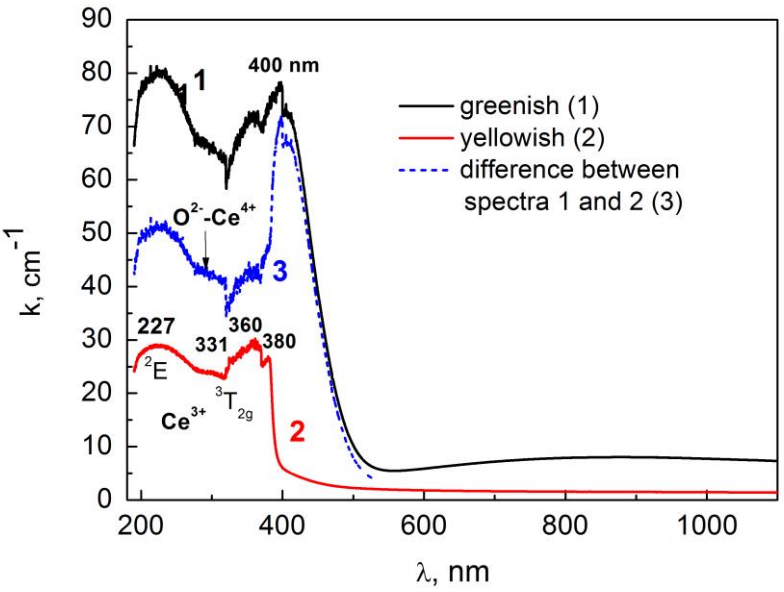

Fig. 6. Absorption spectra of $CeAlO_3$ crystals with different colors. Curve 3 shows differences between the spectra of green and yellowish crystals, probably due to $Ce^{3+} \leftrightarrow Ce^{4+}$ recharging.

The EFG grown crystals consist of perpendicularly-oriented domains. Fig 7a shows the sample annealed in vacuum, which volume consists of randomly oriented domains. On heating of green polished samples the domain boundaries disappeared at 357 K and a new pattern was formed on cooling. On heating of crystals up to 393 K and subsequent cooling the rearrangement of domains

was observed. The boundaries were situated in the (100) and (010) planes with a step of 2-100 μm. The formation of such boundaries worsens crystal transmission if they are not oriented perpendicular to the sample surface.

In yellowish crystals annealed in a reducing atmosphere (Fig. 7b), the boundaries in (100) and (010) plates disappeared at 308 K and new ones formed on (110) and ($\bar{1}$10) planes. The latter persisted on heating up to 473 °C. The different behavior of domains in green and yellow samples we attribute to cerium valence change or presence of admixtures shifting phase transition temperatures.

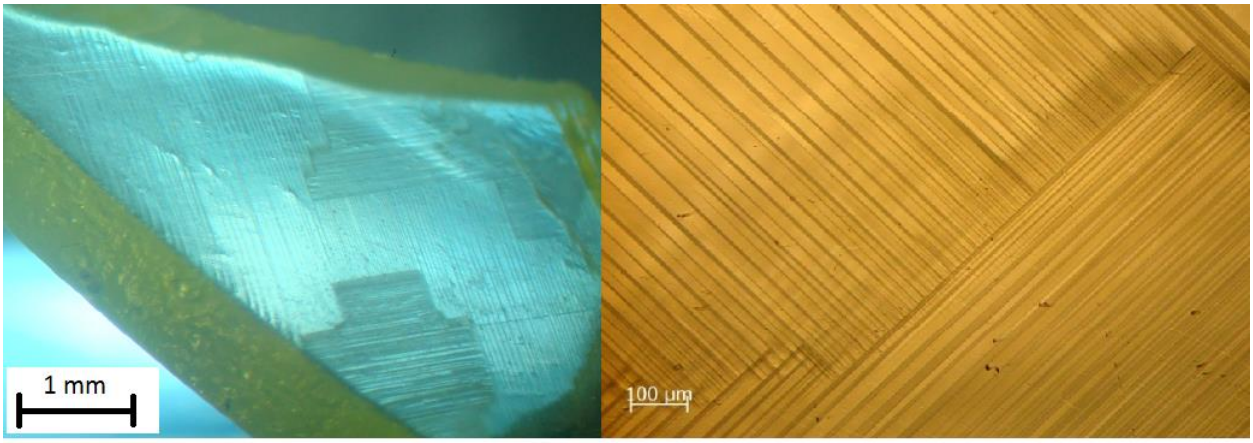

Fig. 7. Domain boundaries in $CeAlO_3$ crystal in transmitted light (description is in text): a - annealed in vacuum, b – annealed in reducing atmosphere.

4.2. Luminescent properties

The majority of grown bulk crystals did not demonstrate bright luminescence under photo excitation, while none of them emitted under X-rays. The complex luminescence band peaked at 375 nm was observed in photoluminescence spectra of green $CeAlO_3$ crystals under excitation at

260 nm range (Fig. 8, a). The two emission bands peaked at 375 and 415 nm can be related to the $5d^1$-4f ($^2F_{5/2,7/2}$) radiative transitions of Ce^{3+} ions in $CeAlO_3$. Indeed, the excitation spectra of Ce^{3+} luminescence registered at 379 nm (curve 1) and 450 nm (curve 2) show typical three band structure in the 230-335 nm range with the main peak at 273 nm, caused by the 4f-5d($^3T_{2g}$) transition of Ce^{3+} ions in the perovskite host. The emission spectra (curves 1 and 2) and excitation spectra (curve 4) of $CeAlO_3$ crystals are significantly shifted from the YAP:Ce counterpart (curves 3 and 5). The excitation spectra of long wavelength luminescence at 450 nm (curve 1) also contain the low intensity band peaked at 373 nm strongly overlapped with the Ce^{3+} emission band in $CeAlO_3$ crystals.

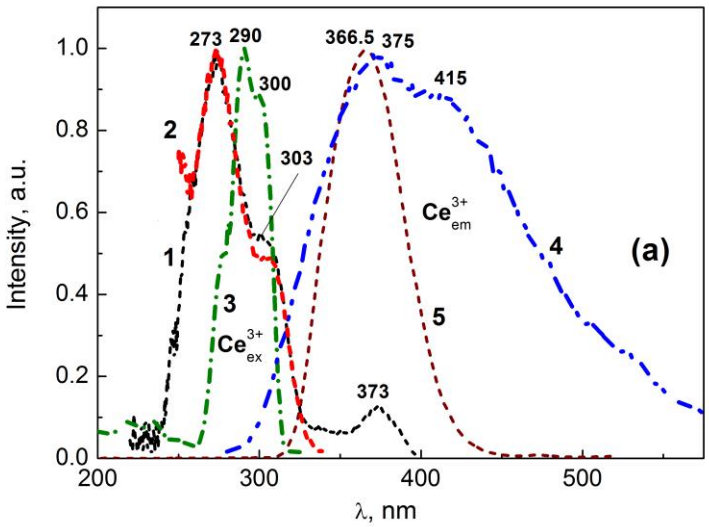

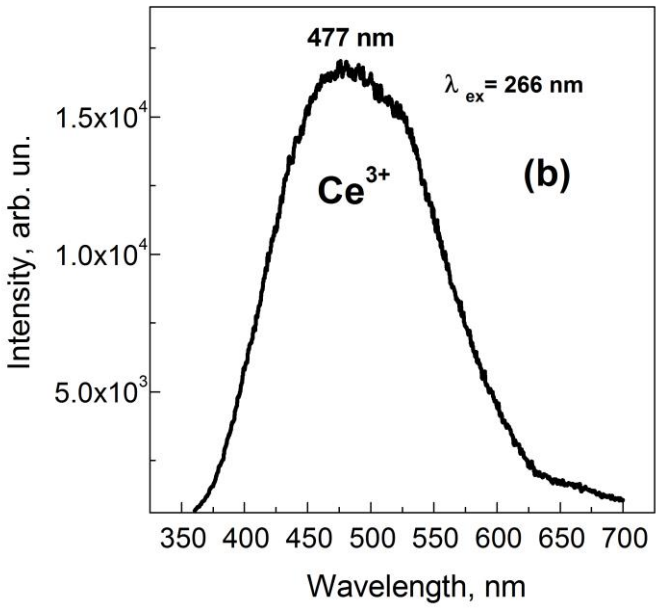

Fig. 8. (a): Excitation (1 – λ_{em} = 450 nm, 2 - λ_{em} = 370 nm) and emission spectra (4 - λ_{ex} = 265 nm) of green $CeAlO_3$ single crystal in comparison with excitation (3 - λ_{em} = 360 nm) and emission (5 - λ_{ex} = 290 nm) of YAP:Ce single crystal. (b): Luminescence spectrum of $CeAlO_3$ skeleton crystals at λ_{ex} = 266 nm.

Taking into account the positions of the low-energy excitation band at 301 nm and strong emission band at 375 nm (Fig.8), the Stokes shift of Ce^{3+} luminescence in the $CeAlO_3$ host can be estimated as 0.812 eV. Such a large Stokes shift of the Ce^{3+} emission in $CeAlO_3$ in comparison with the corresponding value of 0.749 eV in YAP:Ce indicates the increase of the crystal field strength in the cube-octahedral position of the perovskite host where large Ce^{3+} ions are localized.

It is important to note here that the luminescence in the long wavelength spectral range (>450 nm) was also observed in transparent skeleton crystals deposited from the gaseous phase (see Fig. 3a). Namely, under 266 nm excitation these crystals show an intense complex luminescence band in the blue-yellow spectral range peaked at 476 nm (Fig.8b). Previously such luminescence under photoexcitation was also reported in $CeAlO_3$ crystals [19]. It was suggested that not the host, but the admixture $CeAl_{11}O_{18}$ phase is responsible for this emission. However, this compound melts incongruently and cannot be obtained by direct crystallization from the melt.

We have not recognized any admixture phases in the bulk of $CeAlO_3$ single crystals at room temperature, but lines similar to the XRD card for $LaAl_{11}O_{18}$ (34-0467) were discovered in the synthesized raw material and in the opaque surface layer of the EFG grown crystals. These lines are assumed to result from isostructural $CeAl_{11}O_{18}$, which is absent in the XRD database. Hence the observed long wavelength luminescence in both raw material and colored single crystals can be caused by the presence of $CeAl_{11}O_{18}$. We suppose that the concentration of this phase in single crystals is too low to be registered by XRD. Under heat treatment in reducing atmosphere, this phase evidently decomposes and no luminescence is observed thereafter.

At the same time, we cannot exclude here the efficient energy transfer between $CeAlO_3$ and $CeAl_{11}O_{18}$ hosts. Under this assumption, the emission band of Ce^{3+} ions in $CeAlO_3$ peaked at 375 nm can strongly overlap the excitation band of Ce^{3+} luminescence in $CeAl_{11}O_{18}$ peaked at 373 nm.

The latter assumption is supported also by the investigation of PL decay kinetics of $CeAlO_3$ crystals (Fig. 9). Green $CeAlO_3$ crystals under UV excitation at 264 nm demonstrate fast non-exponential decay of luminescence at 350 nm with an average decay time of 20 ns (Fig. 9, curve 1) most probably due to energy transfer from the excited state of Ce^{3+} ions in $CeAlO_3$ to the Ce^{3+} ions in $CeAl_{11}O_{18}$. Under 371 nm excitation, the green $CeAlO_3$ crystals show luminescence in the 460-500 nm range with decay time of 38-43 ns presumably caused by the intrinsic 5d-4f radiative transitions in Ce^{3+} ions in $CeAl_{11}O_{18}$.

However, due to concentration quenching, no luminescence has been registered in $CeAlO_3$ crystals under X-ray excitation at 300 K. Luminescence mechanisms in these crystals have to be specified in further work.

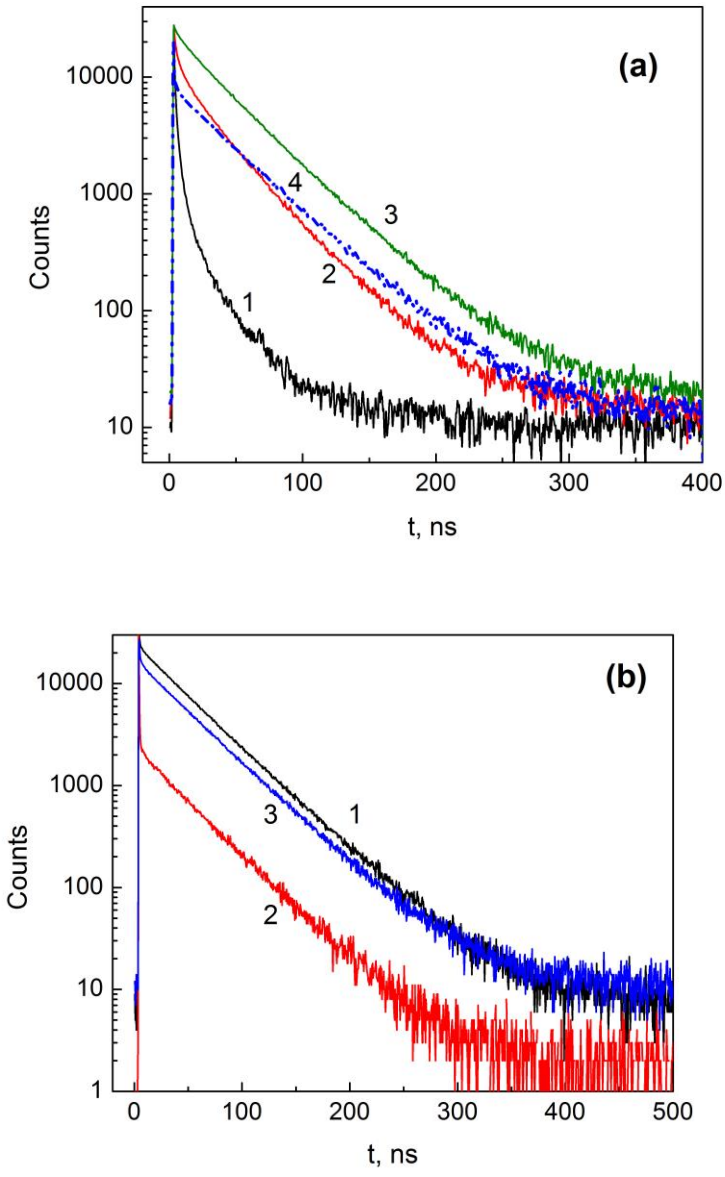

Fig. 9. (a): Luminescence decay kinetics of $CeAlO_3$ crystals under UV-excitation at 264 nm (1- λ_{em} = 350 nm, τ_1 = 1.7 ns, τ_2 = 20 ns; 2 - λ_{em} = 400 nm, τ_1 = 13.6 ns, τ_2 = 33, 3 - τ = 38 ns; 4 – τ = 41 ns); (b): Luminescence decay kinetics of $CeAlO_3$ crystals under UV-excitation at 371 nm (1 - λ_{em} = 485 nm, τ = 43 ns; 2 - λ_{em} = 415 nm, τ = 42 ns; λ_{em} = 550 nm, τ = 43 ns).

4.3. Electrical and magnetic properties

During optimization of the $CeAlO_3$ raw material synthesis procedure, a ceramic sample of gray-rose color was obtained containing some excess of cerium ($Ce_{1,05}Al_{0,95}O_3$) and 2% of carbon admixture. This ceramic has p-type conductivity determined by the sign of thermo EMF. Electric resistance of plate samples with 3 mm thickness was 300 Ω. This result opens a possibility to obtain conductive $CeAlO_3$ ceramics [20, 21]. The nature and mechanism of the observed conductivity needs further study.

Cerium perovskite crystals possess paramagnetic properties. Temperature dependence of inverse magnetic susceptibility χ^{-1} for single- and polycrystalline samples measured in H = 10 Oe magnetic field is plotted versus temperature (Fig. 10). Magnetic susceptibility above 100 K follows the Curie-Weiss law $\chi = C / (T — T_C)$, where C is the Curie constant and T_C is the Curie temperature. Below 100 K, the χ^{-1} (T) the plot deviates from the Curie-Weiss law, evidently, due to some magnetic ordering.

The C and T_C parameters were derived by approximation of experimental data with the Curie-Weiss law (Fig. 11, solid line). For the polycrystalline sample T_C = 45.6 K, while for the single crystal T_C = 35.5 K. The effective magnetic moments of cerium ion determined from the Curie constants are equal to $2.51\mu_B$ and $2.29\mu_B$ for polycrystalline and single crystalline samples, correspondingly. The obtained values are in good agreement with data from [22] and are close to the theoretical value of $2.5\mu_B$ for Ce^{3+} ion calculated by Hund's rule.

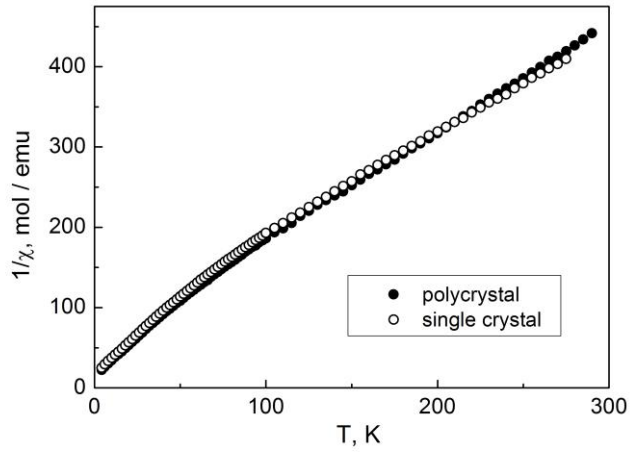

Fig. 10. Temperature dependence of inverse magnetic susceptibility χ^{-1} of polycrystalline (•) and single crystalline (○) $CeAlO_3$.

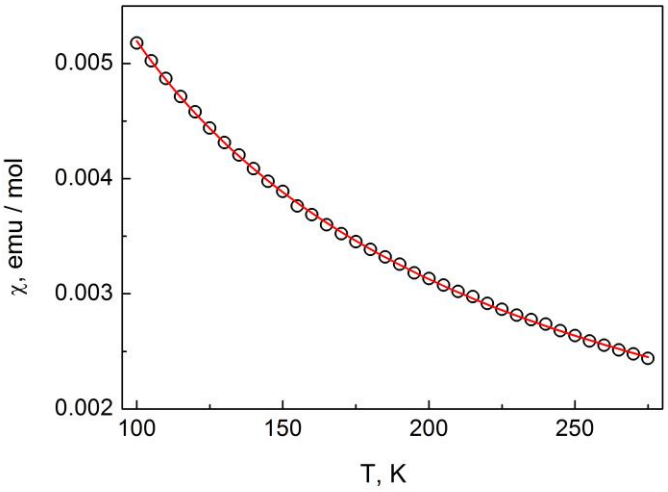

Fig. 11. Temperature dependence of magnetic susceptibility χ of $CeAlO_3$ single crystal above 100 K. Line is an approximation of the experimental data with the Curie-Weiss law.

5. Conclusions

Large $CeAlO_3$ crystals with dimensions up to 130 mm were obtained first time by the Czochralski and EFG techniques. The crystals belong to the tetragonal low temperature modification of $CeAlO_3$, space group P4/mmm, a=3.7669Å, c=3.7967Å. Thermal annealing procedures were developed to minimize coloration and improve optical transparency of crystals. The obtained results show the feasibility of growing shaped $CeAlO_3$ crystals in the form of rods, plates, tubes, cylinders, etc. The developed process can be applied to creation of cost-efficient technologies for obtaining other rare earth aluminate single crystals using inexpensive W and Mo crucibles and crystallizer components.

Ceramic samples and colored $CeAlO_3$ single crystals demonstrate luminescence peaked at 450-475 nm with decay times in the 38-43 ns range. It was attributed to the presence of a $CeAl_{11}O_{18}$ admixture in the samples. This luminescence is strongly excited by the Ce^{3+} radiative transition in the $CeAlO_3$ host, i.e., the excitation energy can be well transferred from the $CeAlO_3$ host to $CeAl_{11}O_{18}$ inclusions. However, no emission was registered under X-ray excitation. Mechanisms of luminescence in $CeAlO_3$ should be the object of further study.

ACKNOWLEDGMENT

The work is partially supported by the Ukrainian-French PICS project between CNRS (Project No.6598) and National Academy of Sciences of Ukraine (Project F2-2015), Marie Skłodowska-Curie Research, Innovation Staff Exchange Project H2020-MSCA-RISE-2014 No. 644260 “Intelum”, and Polish NCN No 2012/07/B/ST5/02376 project.

REFERENCES

[1] P. Lecoq, A.Annenkov, A. Gektin, M. Korzhik, C. Pedrini, *Inorganic Scintillators for Detector Systems: Physical Principles and Crystal Engineering*; Springer: Heidelberg, Germany, 2006.

[2] G. Dhanaraj, K. Byrappa, V.Prasad, M. Dudley, *Springer Handbook of Crystal Growth*: Springer Science & Business Media: Heidelberg, Germany, 2010.

[3] L. Vasylechko, A. Senyshyn, U. Bismayer, Perovskite-type aluminates and gallates. In *Handbook on the Physics and Chemistry of Rare Earths;* Gschneidner, K.A. Jr.; Bünzli, J.-C.G; and Pecharsky, V.K., Eds.; Elsevier: Netherlands: North-Holland, 2009; Vol. 39, pp 113-295.

[4] L. Vasylechko, A. Senyshyn, D. Trots, R. Niewa, W. Schnelle, M. Knapp, *J. Solid State Chem.* 180 (2007) 1277–1290.

[5] M. Małecka, L. Kępiński, *Cryst. Eng. Comm*. 17 (2015) 2273-2278.

[6] J. T. S. Irvine, P. Connor, *Solid Oxide Fuels Cells: Facts and Figures, Green Energy and Technology*: Springer-Verlag, London 2013.

[7] A. Shekykh, B. Melekh, *Phys. Solid State* 45 (2003) 248-252.

[8] M. Tanaka, T. Shishido, H. Horiuchi, N. Toyota, D. Shindo, T. Fukuda, *J. Alloys Compd*. 192(1993) 84-86.

[9] T. Shishido, S. Nojima, M. Tanaka, H. Horiuchi, T. Fukuda. *J. Alloys Compd*. 227 (1995) 175-179.

[10] T. Shishido, S. Okada, K. Kudou, K. Nakajima, *Pac. Science Rev.* 10 (2008) 45-48.

[11] V. Desnenko, A. Panfilov, A. Smirnov, *Phys. Nizk. Temp*. 21(1995) 546–552.

[12] A. Fedorchenko, V. Lyakhno, V. Shnyrkov, *Problems of Atomic Science and Technology*, 1 (2010) 150-156.

[13] M. Mizuno, R. Berjoan, J. Coutures, Foex, M., International Solar Energy Society Congress, Los Angeles, California, July 28-August 1, 1975.

[14] P. Arhipov, S. Tkachenko, S. Vasyukov, M. Biatov, O. Sidletskiy, P. Mateychenko, E. Bryleva. *Func. Mater*. 21 (2014) 472-475.

[15] S. Turczynski, K. Orlinski, D. Pawlak, R. Diduszko, J. Mucha, M. Pekala, J. Fagnard, P. Vanderbemden, and M. Carpenter. *Cryst. Growth Des*., 11 (2011) 1091–1097.

[16] A. Feteira, M. Lanagan, D. Sinclair, *J. Appl. Phys*., 101 (2007) 064110.

[17] A. Cuneyt Tas, M. Akinc, *J. Am. Chem. Soc*. 77 (1994) 2961-2967.

[18] Y. Zorenko, V. Gorbenko, I. Konstankevych, T. Voznjak, V. Savchyn, M. Nikl, J. Mares, K. Nejezchleb, V. Mikhailin, V. Kolobanov, D. Spassky, *Rad. Meas*., 42 (2007) 528-532.

[19] L. Yin, G. Chen, C. Wang, X. Xu, L. Hao, H. Hintzen. *ECS Journ. Solid State Sci. Technol.* 3 (2014) 131-138.

[20] S. Venâncio, P. Miranda, . *Scr. Mater*. 65 (2011) 1065–1068.

[21] T. Ishihara, *Perovskite Oxide for Solid Oxide Fuel Cells* Ed.; Springer: Dordrecht Heidelberg London New York, 2009.

[22] S. Okada, K. Kudou, K. Iizumi, K. Nakajima, T. Shishido, *Transactions of the Kokushikan Univ. Science and Engineering*, 1 (2008) 43-45.